Investigation on the Mechanism of Nanodamage and Nanofailure for Single ZnO Nanowires under an Electric Field

Peifeng Li,[†,‡] Qingliang Liao,[†,‡] Zheng Zhang,[†] Zengze Wang,[†] Pei Lin,[§] Xiaohui Zhang,[†] Zhuo Kang,[†] Yunhua Huang,[†] Yousong Gu,[†] Xiaoqin Yan,[†] and Yue Zhang*[,†,§]

[†]Key Laboratory of New Energy Materials and Technologies, School of Materials Science and Engineering and [§]State Key Laboratory for Advanced Metals and Materials, University of Science and Technology Beijing, 100083 Beijing, People's Republic of China

Ⓢ *Supporting Information*

ABSTRACT: The electrical service behavior of ZnO nanowires (NWs) with various diameters was investigated by a nanomanipulation technique. The nanodamage and nanofailure phenomena of the ZnO NWs were observed when external voltages were applied. The threshold voltages of the ZnO NWs increased linearly from 15 to 60 V with increasing diameter. The critical current densities were distributed from 19.50×10^6 to 56.90×10^6 A m^{-2}, and the reciprocal of the critical current density increased linearly with increasing diameter as well. The thermal core−shell model was proposed to explain the nanodamage and nanofailure mechanism of ZnO NWs under an electric field. It can be expected that the investigation on the nanodamage and nanofailure of nanomaterials would have a profound influence on practical applications of photoelectric, electromechanical, and piezoelectric nanodevices.

KEYWORDS: ZnO NWs, nanomanipulation, nanodamage and nanofailure, thermal core−shell model
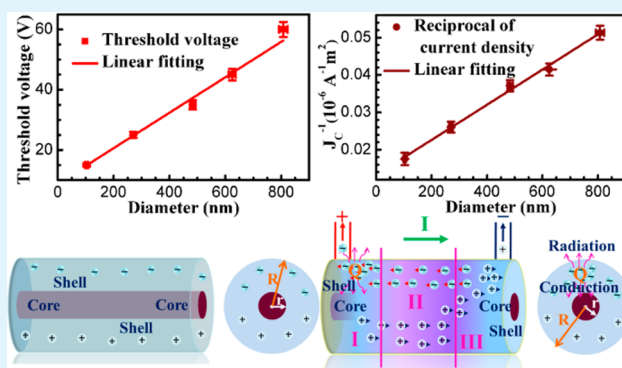
INTRODUCTION

One-dimensional (1D) ZnO nanomaterials such as nanowires (NWs), nanobelts (NBs), nanorods, and nanoarrays are being intensely studied because of their large reserves, easy synthesis, low cost, remarkable semiconducting, electrical, optical, photoelectric, piezoelectric, electromechanical, and chemical properties, biocompatibility, and nontoxicity.[1−5] Numerous prototype nanodevices based on 1D ZnO nanomaterials have been fabricated, such as photoelectric converters, light-emitting diodes, nanolasers, dye-sensitized solar cells, field-effect transistors, nanosensors, nanoelectromechanical systems, nanogenerators,[2−8] and so on.

For the practical application of prototype nanodevices,[9−15] it is necessary to consider their safety, stability, reliability, and durability. Few researchers have observed damage and failure phenomena of ZnO NWs or NBs.[16−27] Wan et al. observed the electrical failure of the single-crystalline ZnO:In NBs under an electric field.[16] Chen and Zhu observed the elastic fracture behavior of ZnO NWs bent by the atomic force microscopy (AFM) tip.[22] Boland et al. observed the fracture of ZnO NWs deposited by a platinum line on the trenches under the pressure applied by the AFM tip.[23] Xu et al. observed the fracture of ZnO NWs by in situ scanning electron microscopy (SEM) tension.[24] Wang et al. observed the chemical corrosion of ZnO NWs interacted with deionized water, ammonia, a NaOH solution, and horse blood serum.[25,26] Electrical, mechanical, and electromechanical damage and failure phenomena were observed in the investigation using nanomanipulation, conductive AFM systems, and in situ transmission electron microscopy (TEM) resonance by our group.[17−21] However, the damage and failure mechanisms have almost no further research in the previous reports. The damage and failure of the nanomaterials would affect the practical application of nanodevices. Thus, it is important and necessary to investigate the threshold value of the damage and failure and the mechanism systematically and deeply.

In this paper, the electrical service behavior of ZnO NWs with increasing diameter under an electric field was investigated. Electrical damage and failure phenomena were observed under an electric field, and some critical parameters were also obtained. The thermal core−shell model was proposed to explain the damage and failure mechanism.

RESULTS AND DISCUSSION

Parts a and b of Figure 1 show the SEM and TEM images of the as-synthesized ZnO NWs, which reveals a large quantity of ZnO NWs with lengths over several tens to hundreds of micrometers and diameters over several tens to hundreds of nanometers. Figure 1c and its inset show the high-resolution TEM (HRTEM) image and the selected area electron
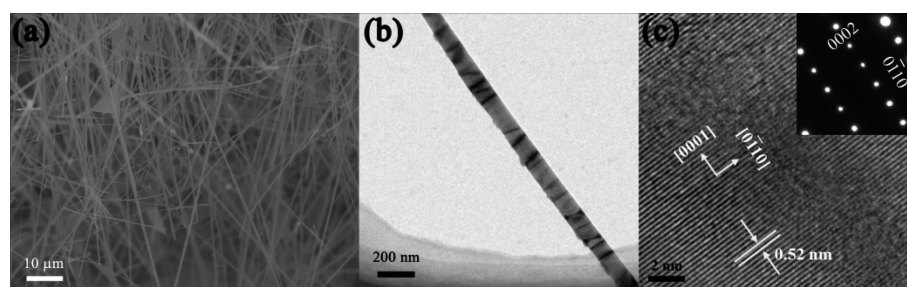
Figure 1. (a) SEM, (b) TEM, and (c) HRTEM images of the ZnO NWs (inset: SAED pattern of the ZnO NW).

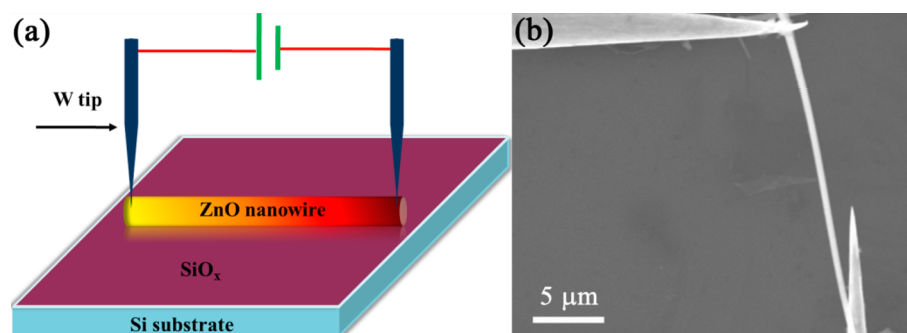**Figure 2.** (a) Electrical characteristic testing schematic diagram and (b) in situ SEM electrical testing image of the single ZnO NW.
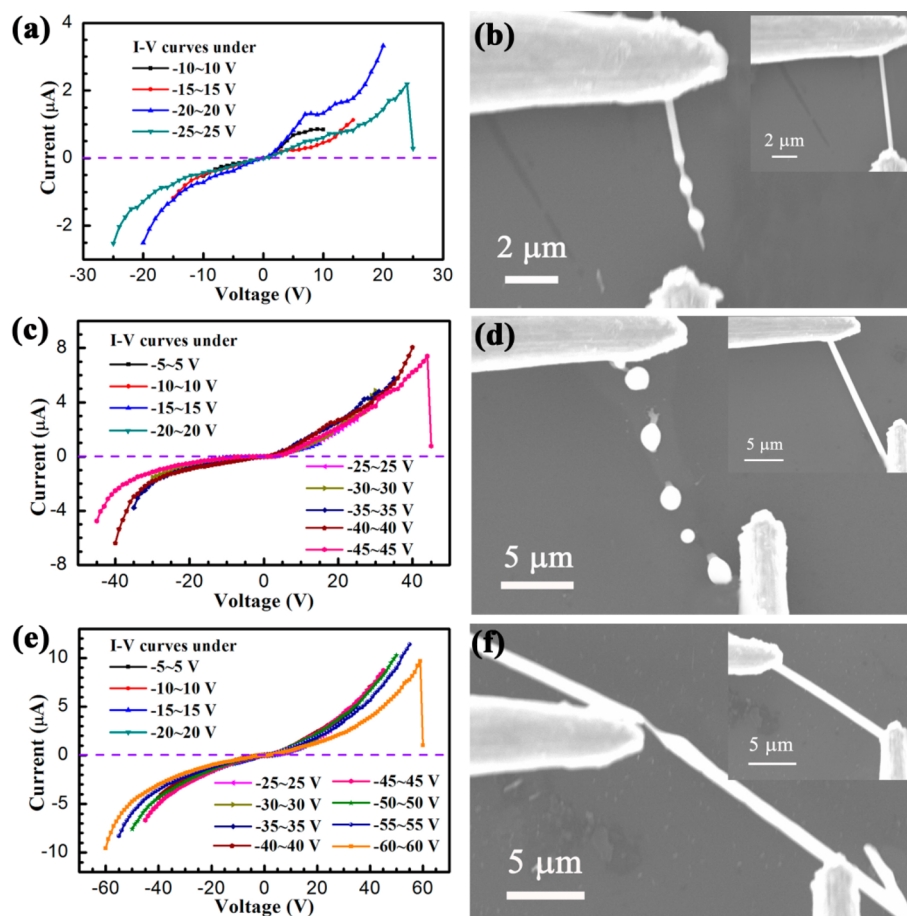

Figure 3. $I-V$ curves of the ZnO NWs with diameters of (a) 270, (c) 625, and (e) 807 nm, respectively. Corresponding in situ SEM images of the three kinds of nanodamaged structures of ZnO NWs under external voltage when the currents drop to 0: (b) broken pearl-like chains; (d) separated pearl-like spheres; (f) necking.

diffraction (SAED) pattern of the ZnO NW, which indicate that the ZnO NW is single crystal and grows along the [0001] direction.

The electrical testing schematic and in situ SEM electrical testing image of the single ZnO NW are shown in parts a and b of Figure 2, respectively. The electrical service behaviors of five single ZnO NWs were investigated by applying longitudinal voltages. The single ZnO NWs with different diameters ranging from 103 to 807 nm (the size of the ZnO NWs used in our experiments is shown in Figure S1 in the Supporting Information) were contacted with the tungsten (W) tips, respectively, and the metal−semiconductor−metal (MSM) structure was formed. Parts a, c, and e of Figure 3 show the I−V curves of ZnO NWs with diameters of about 270, 625, and 807 nm under different voltage ranges. It can be seen that the I−V curves showed obvious dual Schottky characteristics, and the currents suddenly dropped to 0 at certain high voltages. The morphologies of the ZnO NWs were observed when the currents dropped to 0. The damage and failure phenomena that were observed are shown in Figure 3b,d,f. The nanodamage and nanofailure was used to describe the damage and failure phenomena of the nanomaterials, and damage and failure phenomena of ZnO NWs under an electric field belong to electrical nanodamage and nanofailure. The fracture section and vicinity zone of the failed ZnO NW became coarser and thinner even to pearl-like chains from a smooth and uniform surface. Three kinds of typical failure or fracture modes can be classified: (1) broken pearl-like chains (Figure 3b), (2) separated pearl-like spheres (Figure 3d), and (3) necking (Figure 3f).

Under an electric field, Joule heat is generated as a result of the current flowing. The ZnO NW starts to melt when its temperature increases to the melting point induced by Joule heat. The diameters d and corresponding effective lengths l of the ZnO NWs were measured from the inset SEM images in Figure 3b,d,f. The threshold voltages V_{th} and critical currents I_c of ZnO NWs were also obtained from the I−V curves in Figure 3a,c,e. The relationship between the threshold voltage V_{th} and the diameter d is shown in Figure 4a. It can be seen that the threshold voltages of the single ZnO NWs with diameters of 103, 270, 483, 625, and 807 nm were 15, 25, 35, 45, and 60 V, respectively. The threshold voltages of the ZnO NWs increased linearly with increasing diameter.

The critical current density J_c can be calculated by the critical current I_c and the cross-sectional area A of the ZnO NW using the following equation:

$$J_c = I_c/A = I_c/(\pi d^2/4) = 4I_c/\pi d^2 \tag{1}$$

The relationship between the critical current density J_c and the diameter d is shown in Figure 4b. It can be seen that the critical current densities of the single ZnO NWs with diameters of 103, 270, 483, 625, and 807 nm were 56.90×10^6, 38.37×10^6, 26.94×10^6, 24.12×10^6, and 19.50×10^6 A m^{-2}. The critical current density of the ZnO NWs decreased exponentially with increasing diameter, and the reciprocal of the critical current density increased linearly with increasing diameter. The fitted equation of the fitting curve is shown as follows:

$$J_c = 1/(4.708 \times 10^{-5}d + 0.013)$$

$$\text{(range of application: } 103 \text{ nm} \leq d \leq 807 \text{ nm)} \tag{2}$$
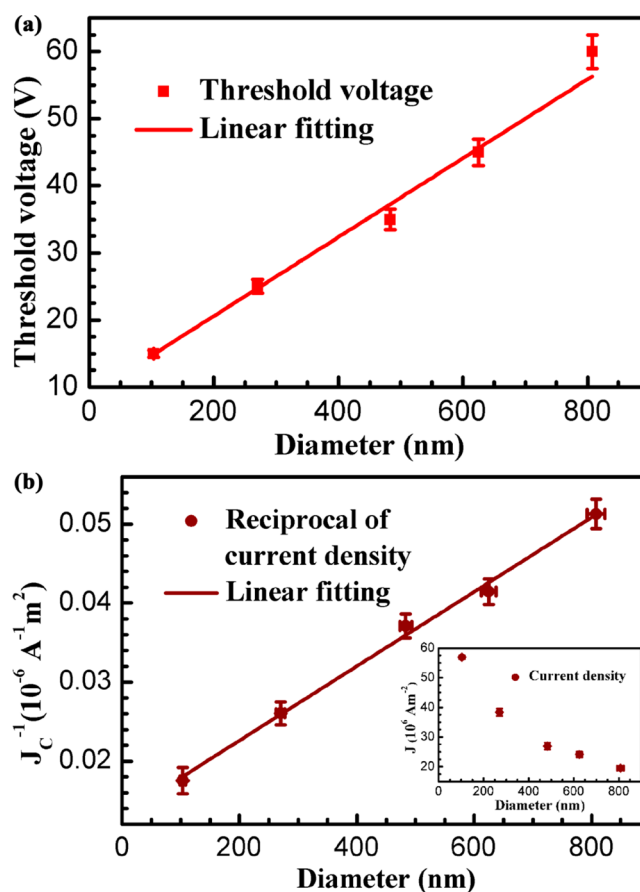

Figure 4. Relationship between (a) the threshold voltages and diameters of ZnO NWs and (b) the critical current densities and diameters of ZnO NWs in the MSM structure.

The threshold voltage and critical current density can be used as the evaluation and criterion to judge the work state of the ZnO NWs as the building blocks integrated in nanodevices.

When an external voltage is applied on the single ZnO NW, Joule heat is generated as a result of the current flowing. Moreover, heat loss occurs because of heat conduction, conversion, and radiation. Joule heat is generated and accumulated gradually, and the temperature of the ZnO NW is also increased with increasing time. Damage or failure occurs when the temperature exceeds the melting point of ZnO NWs. According to Joule's law, Joule heat Q generated in the ZnO NW can be calculated by

$$Q = VIt \tag{3}$$

The heat flux q is the heat through a cross section with unit area in unit time. Assuming that all of the heat is conducted through the end of the ZnO NW, it can be calculated by

$$q = Q/(At) = VIt/[(\pi d^2/4)t] = 4VI/\pi d^2 \tag{4}$$

The value of VI in eq 4 can be obtained by calculating the area between the I−V curve and x axis ($y = 0$). The heat-generating rate Q' is the heat generated through a cross section in unit time. It can be expressed as

$$Q' = Q/t = VI \tag{5}$$

The dependences of the generated heat flux and heat-generating rate on the diameters of the ZnO NWs are shown by the purple line in Figure 5a,b. Because of the vacuum
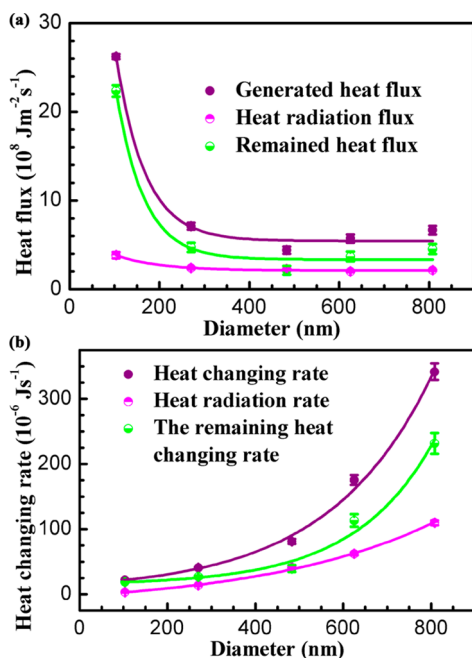
Figure 5. (a) Relationship between the heat flux (generated heat flux, heat radiation flux, and remaining heat flux) and the diameters of ZnO NWs. (b) Relationship between the heat changing rate (heat-generating rate, heat radiation rate, and remaining heat changing rate) and the diameters of ZnO NWs.

environment in SEM and the line contact between the ZnO NW and insulated SiO_x substrate, heat conversion and conduction could be neglected. So, thermal radiation is the main source of heat loss. Although the emissivity ε of the ZnO NW is unknown, the largest heat radiation rate can be calculated by the Stefan−Boltzmann law with $\varepsilon = 1$. In order to simplify the calculations, the radiation temperature is always selected as the bulk melting point:[27]

$$Q_r' = \sigma S T_m^4 \tag{6}$$

$\sigma = 5.67 \times 10^{-8}$ W m^{-2} K^{-4} is the Stefan−Boltzmann constant, $S = \pi dl$ is the radiation area of the ZnO NW, and T_m is the melting point of the ZnO NW. According to eq 6 with $T_m =$ 2248 K, the heat radiation rate and remaining heat rate ($Q' - Q_r'$) are calculated and shown by the pink and green lines in Figure 5b, respectively. The remaining heat (changing rate) is used to heat and melt the ZnO NW until it fractures. By using the melting points, the heat radiation flux on the surface of the ZnO NW can be calculated by

$$q_r = \sigma T_m^4 \tag{7}$$

Because of the difference between the surface area and cross-sectional area of the ZnO NWs, the heat radiation flux should be transformed into an equivalent heat radiation flux in the cross section.

$$q_{r-c} = \pi dl q_r / (\pi d^2 / 4) = 4l q_r / d \tag{8}$$

The dependences of the heat radiation flux and the remaining heat flux ($q - q_{r-c}$) on the diameters of the ZnO NWs are shown by the pink and green lines in Figure 5a. From Figure 5, the generated heat flux, heat radiation flux, and remaining heat flux have an approximate exponential decrease with increasing diameter, while the heat-generating rate, heat

radiation rate, and remaining heat changing rate have an approximate exponential increase with increasing diameter. The geometrical and electrical parameters of the ZnO NWs are summarized in Table S1 in the Supporting Information.

Figure 6a shows the energy band diagrams of the W−ZnO NW−W structure when the external voltage V ($V = V_R + V_a +$
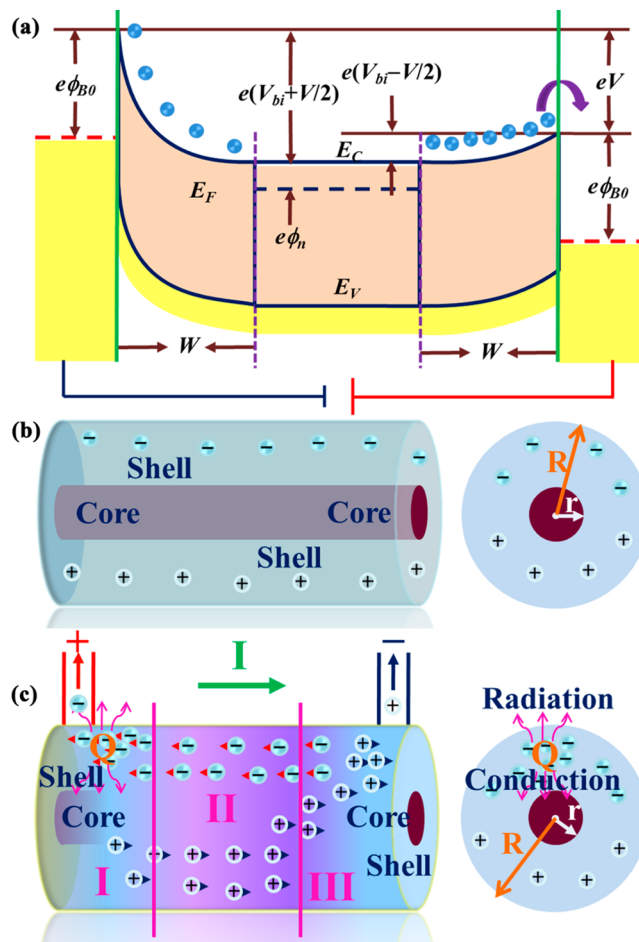

Figure 6. (a) Energy band diagram of an almost symmetric Schottky characteristic ZnO MSM structure under an external voltage. The bias dropped on the left side, and the right side is equal ($V = V_R + V_a + V_{NW}$, where V_R, V_a, and V_{NW} are the reverse bias, positive bias, and bias on the ZnO NW, respectively). The running states of electrons and holes in the ZnO NW with thermal core−shell model: (b) without and (c) under the longitudinal voltage.

V_{NW}, where V_R, V_a, and V_{NW} are the reverse bias, positive bias, and bias on the ZnO NW, respectively) is applied. Owing to the different barrier heights of the W and ZnO NW, electrons flowing from the semiconductor to the metal would accumulate in the space charge region before jumping over the barrier at the metal−semiconductor (MS) junction. Because of the accumulation and collision of electrons and recombination of electrons and holes, more Joule heat would be generated in the MS junctions than other regions when the external voltage is less than 10−20 V.[28−32] When the external voltage exceeds 20 V, the bias dropped on the ZnO NW is dominant compared with the bias dropped on the MS junction. However, the MS junction is also the weak site in the MSM structure, especially the moment when the external voltage is applied, which leads to most of the failures that occurred at the MS junction. All

kinds of failure modes observed in the SEM images of Figure 3 confirmed the above analysis.

As the external voltage increases, more Joule heat is generated, which leads to melting of the ZnO NWs. If Joule heat is generated and distributed uniformly in the whole cross section of the ZnO NW, the inner layer of the ZnO NW would be melted earlier than the outer layer considering that more heat radiates on the surface than in the inner layer. From Figure 3f, it can be seen that the outer layer of the ZnO NW is melting while the inner layer does not fracture. The vicinity diameter of the fractured ZnO NW in Figure S2a in the Supporting Information changes with the uniform gradient, while the original ZnO NW has a uniform diameter. The critical currents leading to the fracture of the ZnO NWs are lower than the next-to-last tested current, which indicates that the resistances of the ZnO NWs tested in the last cycles increase higher than before. The resistance-increasing phenomena imply that the diameters of the ZnO NWs become thinner after the next-to-last test. The morphology of the gradient diameter of the fractured ZnO NW and the critical current reduction phenomena reveal that Joule heat generation and distribution is not uniform within the radial plane of the ZnO NWs. The core−shell model is considered to explain the observed failure phenomena.[33−35] Similar to the mechanical core−shell model of single-crystal ZnO NW established by Zhu's group,[36] we proposed the thermal core−shell model of the single-crystal ZnO NW to explain the Joule heat generation. Figure S3 in the Supporting Information shows the schematic diagram of the mechanisms responsible for the conductance change when the ZnO NW is bent. Owing to the piezoelectric characteristic of the ZnO NW, polarization charges would accumulate on the surface (shell layer) of the ZnO NW when the ZnO NW is bent by the W tip[1,2] (Figure S3a in the Supporting Information), while the core of the ZnO NW has few carriers. Moreover, more electrons would accumulate on the surface of the junction formed by the ZnO NW and W tip when external voltages are applied. The schematic diagrams of the polarization charge distribution are shown in Figure S3b,c in the Supporting Information. Naturally, more Joule heat generates in the shell layer (especially the junction area) of the ZnO NW because of the accumulated electrons in the interface of the junction, which promotes the buildup of the thermal core−shell model.

The schematic diagrams of the thermal core−shell model are shown in Figure 6b,c. In the thermal core−shell model, the ZnO NW in the radial direction is divided into two layers: the outer shell layer with a thickness of $R-r$ and the inner core with a radius of r. Most of the carriers of the ZnO NWs move in the outer shell layer, and Joule heat generates in the transportation of the carriers, while the inner core has little contribution to the carrier movements or the Joule heat generation. When no external voltage is applied, electrons and holes in the shell distribute uniformly and run randomly, as shown in Figure 6b. When an external voltage is applied, the distribution and transportation of electrons and holes start to move regularly, as shown in Figure 6c. Under the influence of an external voltage, electrons move to the positive electrode, while holes move to the negative electrode. The MSM structure can be divided into three regions: I, the MS junction in the positive electrode that accumulates a large number of electrons; II, the center of the ZnO NW in the length direction; III, the MS junction in the negative electrode that accumulates a large number of holes. In region I, a large amount of Joule heat is generated that is attributed to the accumulation and collision derived from electrons. In region II, little Joule heat is generated owing to few collisions of electrons. In region III, little Joule heat is generated because of few recombinations. It concludes that the nanodamage phenomena mainly occur in region I rather than in region II or region III. The SEM images in Figure 3b,d,f confirmed the above conclusion.

The majority of generated Joule heat in the shell layer is conducted to the inner core, which leads to the rise of the temperature of the ZnO NW, while the rest of Joule heat is radiated to the vacuum medium. When the temperature exceeds the melting point, the ZnO NW starts to melt. If the temperature of the shell layer reaches the melting point but the core does not, the shell melts while the core still exists (Figure 3f). If the temperature of the shell and core both reach the melting point, the ZnO NW melts into two or more parts (Figure 3b,d). The melted shell would recrystallize with the rapid loss of heat when an external voltage is removed, and the core with lower temperature is the natural nucleation center. In order to consume heat faster, the morphology of the recrystallized ZnO NW turns out to be pearl-like chains that possess larger specific surface areas.[19] In summary, the main reason for the nanodamage of ZnO NWs is Joule heat generated at the MS junction of the MSM structure because of electron accumulation and collision.

■ CONCLUSIONS

In summary, the concept of nanodamage and nanofailure of nanomaterials was proposed. The electrical service behavior of ZnO NWs with diameters ranging from 103 to 807 nm was investigated by nanomanipulation technique. The nanodamage and nanofailure of the single ZnO NWs were observed when external voltages were applied. The threshold voltages of the single ZnO NWs with diameters of 103, 270, 483, 625, and 807 nm were 15, 25, 35, 45, and 60 V, respectively, and the corresponding critical current densities were 56.90×10^6, 38.37×10^6, 26.94×10^6, 24.12×10^6, and 19.50×10^6 A m^{-2}. The threshold voltages increased linearly with increasing diameter, and the critical current densities decreased exponentially with increasing diameter. The threshold voltage and critical current density can be used as the evaluation and criterion to judge the work state of the ZnO NWs for building nanodevices. The thermal core−shell model was proposed to explain the electrical nanodamage and nanofailure mechanism of ZnO NWs. The main reason for the nanodamage or nanofailure of the ZnO NWs is attributed to Joule heat generated on the surface of the MS junction, which melts the ZnO NW once the temperature exceeds the melting point. The investigation focused on the electrical nanodamage and nanofailure of nanomaterials is necessary and promising for practical applications of photoelectric, electromechanical, and piezo-electric nanodevices.

■ EXPERIMENTAL SECTION

ZnO NWs were synthesized by chemical vapor deposition, which has been described in detail in our previous papers.[37,38] The morphologies were observed by a scanning electron microscope (JEOL-6490). The magnified morphology of the ZnO NW was observed by a transmission electron microscope (Tecnai F30), and the SAED pattern was also obtained.

The electrical service behavior of single ZnO NWs was measured by nanomanipulation and the measurement system for SEM. First, ZnO NWs were ultrasonicated in an ethanol solvent and dispersed on a silicon wafer covered by a 500-nm-thick SiO$_x$ layer in the case of current leakage. Then, the electrical service behavior was carried out in

a scanning electron microscope, which is equipped with a Zyvex S100 nanomanipulation system. The nanomanipulator has four individual probes, and each probe can move independently in the X, Y, Z directions by motors in coarse mode and piezoelectric actuators in fine mode. W tips with ~50 nm radius at the top of each hand were precleaned in isopropyl alcohol to remove the surface oxidation layer in order to serve as a probe to achieve electrical contact with ZnO NWs. A Keithley 4200-SCS instrument equipped with a preamplifier was employed for longitudinal voltage application and current measurement. In the measurement process, the electron gun was shut down to eliminate the influence of electron irradiation. The situation of the ZnO NW (intact or fracture) was observed when the applied voltage was removed. If the ZnO NW was still intact, a bigger voltage range was applied on the ZnO NW and the above procedure was reimplemented until the ZnO NW was fractured; simultaneously, a series of critical parameters were obtained.

■ ASSOCIATED CONTENT

Ⓢ Supporting Information

Size of the ZnO NWs in our experiments, geometrical and electrical parameters, morphology of the fractured ZnO NW, current reduction phenomena, and schematic diagrams showing the mechanisms responsible to the conductance change when the ZnO NW is bent. This material is available free of charge via the Internet at http://pubs.acs.org.

■ AUTHOR INFORMATION

Corresponding Author
*E-mail: yuezhang@ustb.edu.cn.

Author Contributions
‡These authors contributed equally to this work.

Notes
The authors declare no competing financial interest.

■ ACKNOWLEDGMENTS

■ REFERENCES

(1) Wang, Z. L.; Song, J. H. *Science* **2006**, *312*, 242−246.
(2) Wang, X. D.; Zhou, J.; Song, J. H.; Liu, J.; Xu, N. S.; Wang, Z. L. *Nano Lett.* **2006**, *6*, 2768−2772.
(3) Wang, X. D.; Summers, C. J.; Wang, Z. L. *Nano Lett.* **2004**, *4*, 423−426.
(4) Arnold, M.; Avouris, P.; Pan, Z. W.; Wang, Z. L. *J. Phys. Chem. B* **2003**, *107*, 659−663.
(5) Hughes, W.; Wang, Z. L. *Appl. Phys. Lett.* **2003**, *82*, 2886−2888.
(6) Zhang, X. M.; Lu, M. Y.; Zhang, Y.; Chen, L. J.; Wang, Z. L. *Adv. Mater.* **2009**, *21*, 2767−2770.
(7) Qin, Z.; Liao, Q. L.; Tang, L. D.; Zhang, X. H.; Zhang, Y. *Mater. Chem. Phys.* **2010**, *123*, 811−815.
(8) Yang, Y.; Guo, W.; Wang, X. Q.; Wang, Z. Z.; Qi, J. J.; Zhang, Y. *Nano Lett.* **2012**, *9*, 1919−1922.
(9) Park, W. I.; Yi, G. C.; Kim, J. W.; Park, S. M. *Appl. Phys. Lett.* **2003**, *82*, 4358−4560.
(10) Heo, Y. W.; Tien, L. C.; Kwon, Y.; Norton, D. P.; Pearton, S. J.; Kang, B. S.; Ren, F. *Appl. Phys. Lett.* **2004**, *85*, 2274−2276.
(11) Xiang, J.; Lu, W.; Hu, Y. J.; Wu, Y.; Yan, H.; Lieber, C. M. *Nature* **2006**, *441*, 489−493.
(12) Chen, H. S.; Qi, J. J.; Zhang, Y.; Zhang, X. M.; Liao, Q. L.; Huang, Y. H. *Appl. Surf. Sci.* **2007**, *253*, 8901−8904.
(13) Lee, M. J.; Han, S. W.; Jeon, S. H.; Park, B. H.; Kang, B. S.; Ahn, S. E. *Nano Lett.* **2009**, *9*, 1476−1481.
(14) Chang, Y. K.; Hong, F. C. *Nanotechnology* **2009**, *20*, 235202.
(15) Yang, R. S.; Qin, Y.; Li, C.; Dai, L. M.; Wang, Z. L. *Appl. Phys. Lett.* **2009**, *94*, 022905.
(16) Wan, Q.; Huang, J.; Lu, A. X.; Wang, T. H. *Appl. Phys. Lett.* **2008**, *93*, 103109.
(17) Yang, Y.; Zhang, Y.; Qi, J. J.; Liao, Q. L.; Tang, L. D.; Wang, Y. S. *J. Appl. Phys.* **2009**, *105*, 084319.
(18) Yang, Y.; Qi, J. J.; Liao, Q. L.; Guo, W.; Wang, Y. S.; Zhang, Y. *Appl. Phys. Lett.* **2009**, *95*, 123112.
(19) Zhang, Q.; Qi, J. J.; Yang, Y.; Huang, Y. H.; Li, X.; Zhang, Y. *Appl. Phys. Lett.* **2010**, *96*, 253112.
(20) Zhang, Y.; Yan, X. Q.; Yang, Y.; Huang, Y. H.; Liao, Q. L.; Qi, J. J. *Adv. Mater.* **2012**, *24*, 4647−4655.
(21) Li, P. F.; Liao, Q. L.; Yang, S. Z.; Bai, X. D.; Huang, Y. H.; Yan, X. Q.; Zhang, Z.; Liu, S.; Lin, P.; Kang, Z.; Zhang, Y. *Nano Lett.* **2014**, xx−xx.
(22) Chen, Q.; Zhu, J. *Appl. Phys. Lett.* **2007**, *90*, 043105.
(23) Wen, B. M.; Sader, J. E.; Boland, J. J. *Phys. Rev. Lett.* **2008**, *101*, 175502.
(24) Xu, F.; Qin, Q. Q.; Mishra, A.; Gu, Y.; Zhu, Y. *Nano Res.* **2010**, *3*, 271−280.
(25) Zhou, J.; Xu, N. S.; Wang, Z. L. *Adv. Mater.* **2006**, *18*, 2432−2435.
(26) Wang, Z. L. *J. Nanosci. Nanotechnol.* **2007**, *8*, 27−55.
(27) Pan, C. L.; Wen, Y. H.; Zhu, Z. Z. *J. Xiamen Univ.* **2007**, *46*, 478−481.
(28) Wang, D.; Lu, J. G.; Otten, C. J.; Buhro, W. E. *Appl. Phys. Lett.* **2003**, *83*, 5280−5282.
(29) Cui, Y.; Duan, X. F.; Hu, J. T.; Lieber, C. M. *J. Phys. Chem. B* **2000**, *104*, 5213−5216.
(30) Chung, S. W.; Yu, J. Y.; Heath, J. R. *Appl. Phys. Lett.* **2000**, *76*, 2068−2070.
(31) Hu, S. F.; Wong, W. Z.; Liu, S. S.; Wu, Y. C.; Sung, C. L.; Huang, T. Y.; Yang, T. J. *Adv. Mater.* **2002**, *14*, 736−739.
(32) Zhang, Z. Y.; Jin, C. H.; Liang, X. L.; Chen, Q.; Peng, L. M. *Appl. Phys. Lett.* **2006**, *88*, 073102.
(33) Namjoshi, K. V.; Mitra, S. S.; Vetelino, J. F. *Phys. Rev. B* **1971**, *3*, 4398−4403.
(34) Lauhon, L. J.; Gudiksen, M. S.; Wang, D.; Lieber, C. M. *Nature* **2002**, *420*, 57−61.
(35) Yang, R. G.; Chen, G. *Nano Lett.* **2005**, *5*, 1111−1115.
(36) Chen, C. Q.; Shi, Y.; Zhang, Y. S.; Zhu, J.; Yan, Y. J. *Phys. Rev. Lett.* **2006**, *96*, 075505.
(37) Huang, Y. H.; Bai, X. D.; Zhang, Y. *J. Phys.: Condens. Matter* **2006**, *18*, 179−184.
(38) Huang, Y. H.; Zhang, Y.; Gu, Y. S.; Bai, X. D.; Qi, J. J.; Liao, Q. L.; Liu, J. *J. Phys. Chem. C* **2007**, *111*, 9039−9043.